Deep Learning Regression for Quantitative LIBS Analysis of Aluminium Scrap

Simon Van den Eynde [a, b,1*], Dillam Jossue Díaz-Romero [a,b,c,1], Isiah Zaplana [a,b], Jef Peeters [a,b]

[a]Department of Mechanical Engineering, KU Leuven, Celestijnenlaan 300, Leuven 3000, Belgium

[b]Core Lab Value, Cost & Circularity in Manufacturing, Flanders Make, Leuven 3000, Belgium

[c]PSI-EAVISE, KU Leuven, Jan Pieter de Nayerlaan 5, Sint-Katelijne-Waver 2860, Belgium

[1] These authors contributed equally.

* Corresponding author: simon.vandeneynde@kuleuven.be

Abstract — ***One of the most promising innovation strategies for sorting and recycling post-consumer aluminium scrap is using quantitative Laser-Induced Breakdown Spectroscopy (LIBS) analysis. However, existing methods to estimate alloying element concentrations based on LIBS spectra, such as linear univariate regression and Machine Learning models, are still too limited in their performance to achieve the accuracy demanded by the industry. Therefore, this study presents novel Deep Learning approaches and compares their performance to those of traditional univariate regression and Machine Learning methods in terms of RMSE, MAE, and R^2 value. For this evaluation, two sample sets of aluminium pieces are used: one containing 27 certified aluminium reference samples and the second containing 733 post-consumer scrap pieces for which the ground truth concentrations are determined by X-Ray Fluorescence (XRF).***

Adopting multiple loss functions, one for each element has proven its significant value for the regression performance. It improves the results for all performance metrics in the Scrap Sample set, and the same is true for the Reference Sample set, except for the coefficient of determination of Fe, Mn and Mg. In addition, the proposed methodology considers the learning prioritisation problem to prevent that learning the concentration of the base element is prioritised over the alloying elements. Although the effect of excluding the base alloy aluminium from the learning is small and not always positive for the performance, demonstrating this effect is also considered valuable. Since the average RMSE on the prediction is just 0.02 wt.% for Al and Si, and not more than 0.01 wt.% for Fe, Cu, Mn, Mg, and Zn, the best performing Deep Learning model shows promise for the future of LIBS in metal sorting applications.

Keywords: *Artificial Intelligence; Metal recycling; Aluminium recycling; Machine Learning; Laser-Induced Breakdown Spectroscopy; Deep Learning; Multi-loss functions; Regression*

1. *Introduction*

The implementation of sorting systems based on Laser-Induced Breakdown Spectroscopy (LIBS) is a priority in the innovation strategy of European Aluminium (EA), the European aluminium industry association [1] [2]. The goal of using LIBS is to sort aluminium post-consumer scrap into recyclable alloy groups. Currently, a downcycling dynamic is dominant, where the collected aluminium post-consumer scrap, typically a mix of various alloys, is mostly used to produce secondary cast alloys [3]. This approach is suboptimal since it is characterised by significant quality losses [4]. The wrought aluminium alloys in the mix of post-consumer scrap typically have a significantly higher purity than the cast alloys, which have relatively high concentrations of alloying elements [5]. However, since nowadays wrought and cast alloys are typically not yet separated, this higher purity is not recovered, resulting in considerable quality losses. Sorting the post-consumer scrap in alloy groups allows for mitigating these quality losses by enabling wrought-to-wrought recycling [6].

A considerable amount of research has recently been dedicated to classifying aluminium alloys using LIBS. The feasibility of classifying aluminium reference samples by their alloy series with high accuracy has been demonstrated in prior research [7] [8]–[10]. The classification of aluminium scrap pieces has been explored as well. However, the used sample sets in previous research are often very small and do not adequately span the entire range of alloys typically present in post-consumer scrap. Campanella et al. (2017) used Artificial Neural Networks (ANN) to classify aluminium scrap samples. However, the data set included only 35 samples of 4 wrought alloy series [11]. Werheit et al. (2011)

Electronic copy available at: https://ssrn.com/abstract=4284144

applied LIBS to distinguish cast from wrought scrap samples [12]. Their data set was relatively large (248 pieces) and representative for post-consumer aluminium scrap. However, in this case, the researchers removed 20% of the samples in the data set with either extremely high or low Si concentrations, in addition to samples with paint or other types of surface contamination.

An industrial application mentioned in the literature review of Legnaioli et al. (2020) is the LIBS system of SECOPTA analytics GmbH [13]. This company has claimed good results when sorting aluminium scrap by alloy series [14]. However, sorting by alloy series is not always interesting from a commercial point of view. Most sensor-based sorting systems have just two or three sorting outputs since the physical separation of the processed material into even more output fractions is technically challenging at high throughputs. Therefore, the authors have previously explored the classification of post-consumer aluminium scrap into three commercially interesting output fractions using LIBS, Machine Learning (ML), and Deep Learning (DL) [9] [10]. A data set of 834 samples was used for this research, constituting a representative mix of post-consumer aluminium scrap. The method made it possible to assign the samples to the selected classes with relatively good accuracy. However, a significant drawback is that the output classes are not flexible. The DL classification method requires an extensive data set of samples assigned to the ground truth classes for training. If the output classes must be modified, the samples in the data set must be assigned to a new ground truth class. Otherwise, the DL classifier cannot be trained. Repeating the assignment of samples to ground truth classes and retraining every time a new sorting task is adopted is not interesting in an industrial context. Therefore, a new strategy is considered for sorting aluminium scrap, one that is more flexible to changes in the sorting task. In addition, the new method is developed to be also more generic in terms of the metal to be analysed. While the previously developed classification approach included a feature extraction step specific to aluminium matrices, the new approach is completely devoid of steps specific to one type of matrix. That way, the new method could be applied to more materials than just aluminium scrap.

The proposed method is based on regression. The strategy is to estimate the concentrations of the alloying elements for each sample and make the sorting decision based on these estimated concentrations, as proposed by other researchers [15] [16] [17]. Regression in the context of LIBS has been studied thoroughly already. The simplest form of regression is linear univariate regression. This approach is frequently applied to estimate alloying element concentrations in aluminium alloys [18] [19] [20] [21], as well as other metals such as copper and steel alloys [22] [23]. It has also been used for the chemical analysis of aluminium oxide and molten primary aluminium [24] [25]. However, this method is particularly susceptible to issues related to matrix effects, which are notorious for complicating quantitative LIBS analysis. Also, for the case of aluminium matrices, matrix effects have been shown to significantly impact the quantitative analysis of alloying elements, such as Si, Mn, and Cu [26]. Other issues, such as signal fluctuations, self-absorption, and spectral overlap of different emissions, also impact the accuracy of this method. Therefore, linear univariate regression is not robust enough for many applications.

A more complex approach is to use Machine Learning methods for regression. Machine Learning methods in the context of LIBS have been used in previous research to estimate trace amounts of impurities and alloying element concentrations in a wide range of applications, such as iron ores [27], coal [28], food [29], soils [30], geological samples [31], electrolytes [32], steel [33], heavy metals [34], rocks [35] [36] [37] [38], and phosphate slurries [39]. Machine Learning algorithms used in these studies include Partial Least Squares (PLS), Least Squares Support Vector Machine (LSSVM), Random Forest (RF), Logistic Regression (RF), and Support Vector Regression (SVR). Regression methods specifically tested for aluminium alloys include Artificial Neural Networks (ANN) [40] [41] [42], Least Squares Support Vector Machine (LSSVM) [43], and multivariate regression [44]. Machine Learning methods can mitigate issues stemming from matrix effects and signal fluctuations and are therefore considered superior to univariate methods [45]. However, in many applications, popular Machine Learning methods still fail to meet the required accuracy.

Electronic copy available at: https://ssrn.com/abstract=4284144

In the few cases where Deep Learning models were developed for quantitative LIBS analysis, they have outperformed traditional Machine Learning models thanks to their ability to learn highly nonlinear functions based on large amounts of training data [46]. In the case of sorting metal scrap, this ability is crucial to achieving the required accuracy in the prediction of alloying element concentrations. This article presents a Deep Learning regression method for estimating alloying element concentrations. The used sample sets consist of aluminium material, but the method is developed so that it should also be applicable for other metals. A key contribution of the methodology is the adoption of multiple loss functions for the multi-task learning problem of estimating the concentrations of several alloying elements. Furthermore, the issue of learning prioritisation is considered in order to prevent that learning the concentration of the base element is prioritised over the alloying elements. The article compares the performance of the developed Deep Learning method to more traditional methods to clarify its added value.

2. *Materials*

2.1. *Samples*

This study used two sample sets: a Reference Sample set and a Scrap Sample set. The first set of 27 certified aluminium reference samples was prepared and provided by the Swedish metals research institute Swerim AB. The certified concentrations of the alloying elements were used as the ground truth concentrations for the samples in this data set to evaluate the performance of the tested regression methods.

The second set of samples consists of 773 aluminium post-consumer scrap samples collected at a large Belgian recycling facility. The post-consumer scrap from which the samples are taken is separated from other materials by magnetic separation, a series of density separation steps, vision-based sorting, and sieving. As a result, this scrap fraction consists almost exclusively of aluminium alloys. Due to the sieving step, the scrap samples have dimensions between 40 and 120 mm. The composition of the Scrap Sample set was measured with an Olympus Vanta handheld X-Ray Fluorescence (XRF) device. The scrap samples were locally cleaned with a rotating cutting tool with a tungsten carbon head and ethanol prior to the XRF measurements [40]. As such, surface contamination was removed to avoid distortion in the measurements.

The Vanta Olympus XRF was selected for the concentration measurements of the scrap samples because of its relatively high accuracy. The median 2σ errors, corresponding to a 95.45% confidence level, on the concentration measurements for Al, Mg, Si, Mn, Cu, Zn, and Fe were 858 ppm, 1081 ppm, 158 ppm, 54 ppm, 16 ppm, 9 ppm, and 76 ppm, respectively. A common alternative to XRF, spark optical emission spectroscopy (spark-OES) [47], was tested to measure the concentrations of the alloying elements. However, the spark-OES measurements on the aluminium scrap pieces had lower accuracy. This was mainly due to the scrap pieces' complex shape, making it challenging to apply the spark-OES measurements correctly. Therefore, the results of the XRF were used in this study. The concentrations of alloying elements measured with this device were used as the ground truth concentrations for the samples in this data set to evaluate the performance of the tested regression methods.

2.2. *LIBS setup*

The LIBS setup used in this study is a custom-made industrial setup developed by the companies SPECTRAL Industries and Redwave. It has five main components: a material feeder, a conveyor belt with a speed of 2 meters per second, the LIBS system, a 4k RGB, and a 2k 3D high-resolution camera. The RGB camera can be used for a pre-sorting step to separate cast and wrought aluminium pieces [33] [34]. The 3D camera is used to synchronize the laser with the moving scrap

Electronic copy available at: https://ssrn.com/abstract=4284144

pieces. The pieces are irradiated in free fall when they reach the end of the conveyor belt, where the LIBS system is positioned. The 40 W laser runs at 10 kHz without warm-up time. It has a focal length of 200 mm and a depth of focus (double Rayleigh length) of 20 mm. The spot size diameter is ca. 100 µm, and the pulse duration is 5 ns. A CMOS camera (4096 x 2160 pixels) serves as the detector. A UV spectrometer (190nm – 440nm) runs at a frequency between 100-200Hz. The system has a resolving power $\left(\frac{\lambda}{\Delta\lambda}\right)$ of 2000. With this setup, 10 to 50 spectra are acquired for all pieces in the Reference Sample set and Scrap Sample set. The spectra are randomly divided into three sets for all the following steps: 70% for training, 10% for validation, and 20% for testing. The experiments are computed on GPUs: NVIDIA RTX3090 24 GB and NVIDIA TITAN 12 GB. A CPU: AMD Ryzen Thread ripper 3990x 64-core with 128 GB DDR4 RDIMM memory is used for the training and testing.

3. *Methods*

This section explains the methodology followed to develop a Deep Learning regression method and compares its performance with more traditional regression methods, namely univariate regression, and two Machine Learning models, commonly used in LIBS. A graphical summary of the followed methodology is shown in Figure 3.1. First, the two data sets (the Reference Sample set and the Scrap Sample set) are collected. The ground truth concentrations of seven alloying elements (Al, Si, Cu, Mg, Mn, Zn, and Fe) are established according to the method described in the *Materials* section for every piece in the two data sets. Secondly, LIBS spectra are acquired for all pieces in the data sets using the described LIBS setup.

The collected spectra are then subjected to several pre-processing steps (filtering, normalisation, and baseline correction). Afterwards, the performance of several regression methods is evaluated to estimate the concentrations of the seven alloying elements. The first evaluated models are traditional regression models frequently used in LIBS, namely linear univariate regression and two Machine Learning methods: Random Forest Regression (RF) and Logistic Regression (LR). Afterwards, the performance of the proposed Deep Learning regression method is evaluated. In addition, several approaches are considered regarding the loss functions of the Deep Learning model and the inclusion of the base element aluminium in the training.

Electronic copy available at: https://ssrn.com/abstract=4284144

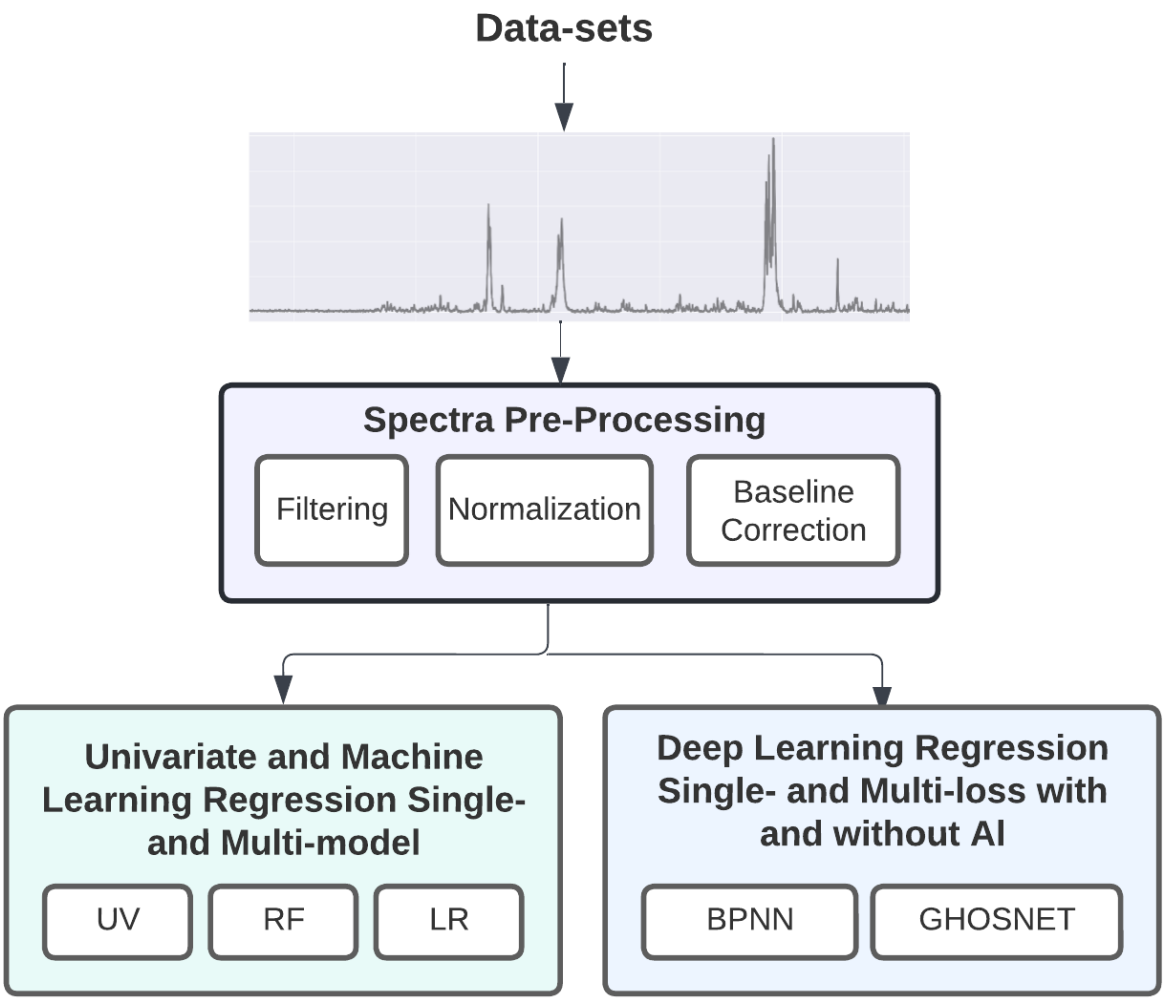

Figure 3.1: Graphical summary regression methodologies

3.1. *Spectra pre-processing (filtering and normalisation)*

As demonstrated in previous research [10], the performance of classification and regression algorithms can benefit from implementing spectral pre-processing steps. Therefore, the collected spectra from both data sets are filtered and normalised according to equations (3 – 1) to (3 – 4). Here, $\{X_1, \dots, X_m\}$ denote the spectra of the pieces with $1 \leq i \leq m$, where m denotes the total number of spectra. For each spectrum X_i:

$$X_i = \{x_j\}_{j=1}^{4096} \tag{3-1}$$

The expression $\{x_j\}_{j=1}^{4096}$ represents the data points of the spectrum X_i. The mean and maximum point of each spectrum are calculated using equations (3 – 2) and (3 – 3), as in previous studies [10].

$$(X_i)_{\text{mean}} = \frac{\sum_{j=1}^{4096} x_j}{4096} X_i \tag{3-2}$$

$$(X_i)_{\max} = \max_j \{x_j\} \tag{3-3}$$

Electronic copy available at: https://ssrn.com/abstract=4284144

Finally, an intensity threshold of T = 1500 counts is set to remove spectra X_i from $\{X_1, \dots, X_m\}$ whose $(X_i)_{\text{mean}}$ is lower than T. Finally, the spectra that are not filtered out are normalised, where $N(X_i)$ denotes the spectrum X_i after being normalised according to equation (3 – 4) [48]:

$$N(X_i) = \frac{X_i}{(X_i)_{\max}} \qquad (3-4)$$

3.2. *Baseline Correction*

Previous studies have shown that the use of a baseline correction can improve the performance of classification and regression algorithms [9], [10], [49]–[51]. LIBS spectra regularly have a significant continuum background and are usually also affected by the detector's dark current [52]. Based on previous research [40], the asymmetric least squares (ALS) smoothing approach introduced by Eilers and Boelens is selected as the baseline correction algorithm for all experiments [53], using the following parameters: the second derivative constraint (λ) equal to 102, the weighting of the positive residuals (p) equal to 10^{-8}, and the number of iterations ($N_{\text{iterations}}$) equal to 20.

3.3. *Univariate regression*

As the name implies, linear univariate (UV) regression is used to estimate a linear relationship between independent variables and dependent variables [54]. This methodology is frequently used to estimate alloying element concentration of metals, plastic, and other materials [18][19][55]. In this study, the UV method was performed for both the Reference Sample set and the Scrap Sample set.

Both cases used the ratio between an alloying element's concentration and the base alloy (aluminium) concentration as the independent variable. The concentrations of aluminium and the alloying elements for the Reference Sample set are known with great accuracy since the sample set consists of certified reference samples. In the case of the Scrap Sample set, the concentrations are measured with the handheld XRF device, which leads to higher uncertainties in the ground truth alloying element concentrations.

The dependent variable is, in both cases, the ratio between the intensity of a selected peak relating to an alloying element and the intensity of a selected peak relating to the base alloy, aluminium. The peaks are selected using the NIST LIBS database [56]. Table 3.1 shows the selected wavelength ranges corresponding to the alloying elements studied in the univariate regression analysis (Al, Si, Cu, Zn, Mn, Mg, Fe). The maximum intensity value within each wavelength region is selected to calculate the intensity ratios for the univariate analysis. This approach is considered more robust than selecting the intensity at a specific wavelength since small wavelength drifts can dramatically affect the analysis results, as demonstrated by Syvilay et al. (2019) [57].

Table 3.1: Wavelength ranges for selected alloying elements

Element	**Al**	**Si**	**Cu**	**Zn**	**Mn**	**Mg**	**Fe**
Wavelength range (nm)	308.0-309.0	287.5-289.0	324.0-325.5	329.9-330.4	402.7-403.8	277.5-278.4	404.2-404.8

Linear univariate regression was performed for the reference and scrap samples for six alloying elements (Si, Cu, Zn, Mn, Mg, and Fe). A linear function is fitted to the data using the "*linregress*" function with the default parameters from the SciPy library in Python, which calculates the best linear fit based on the minimum least-squares algorithm.

Electronic copy available at: https://ssrn.com/abstract=4284144

3.4. *Machine Learning regression*

In addition to the linear univariate regression method, two commonly used Machine Learning models in the field of LIBS are evaluated: Random Forest (RF) Regression [58] and Logistic Regression (LR) [59]. Machine Learning techniques generally perform better than univariate regression in quantitative analysis of alloying element concentrations [60]. Using feature extraction techniques combined with Machine Learning techniques allows to take more information from the spectra into account. The disadvantage is that this method can be more computationally intensive. However, unlike univariate regression, the wavelengths of the intensity peaks corresponding to the relevant alloying elements do not always have to be manually selected.

To assess the performance of the UV model and the Machine Learning models, for both the Reference Sample set and the Scrap Sample set, the library Scikit-learn 1.1.2 in Python was used. The parameters assumed for LR are the default parameters, and the RF parameters are: the number of trees in the forest: 1000, criteria: mse, min_sample_split: 2, bootstrap: True, and oob_score: True. A grid search finds all optimal parameters on the validation set using the following grid search parameters: LR: {'penalty':('l1', 'l2', 'elasticnet', 'none'), 'solver': ('saga', 'lbfgs', 'neewtong-cg', 'sag')}, and RF: {'n_estimators':[100,1000,10000, 50000], 'criterion':('gini', 'entropy', 'rbf ', 'sigmoid ')}, and the parameters not mentioned are set to their default value.

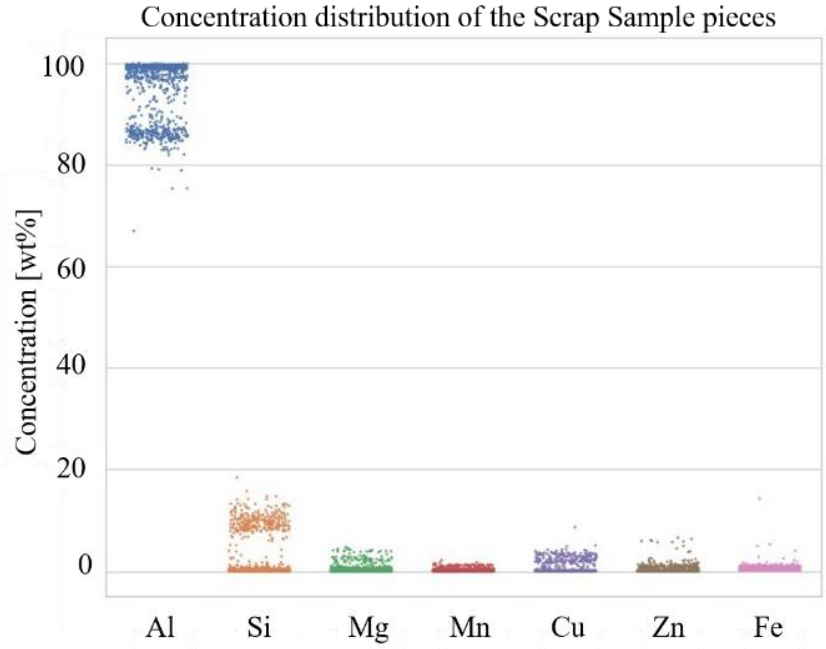

Figure 3.2: Concentration distribution of the Scrap Sample pieces

The concentration distributions for the seven selected elements are shown in Figure 3.2 for the Scrap Sample set. The large difference in concentration between aluminium and the alloying elements could make it challenging to learn all the concentrations well with a single model. The learning in these types of multi-task problems tends to prioritise the easiest tasks, in this case, the element with the highest concentration [61]. To overcome this problem, the authors have considered that Machine Learning techniques can be used to learn the concentrations of alloying elements for all elements together (Single-model) or for each element individually (Multi-model), as shown in Figure 3.3.

In the Single-model approach, the Machine Learning models are trained to estimate all the alloy element concentrations at once, which is represented by the model function F, with each individual

Electronic copy available at: https://ssrn.com/abstract=4284144

submodel denoted by f_i. As a consequence, the learning of the different alloying element concentrations is not independent.

In the Multi-model approach, the selected machine learning models learn only a single element at a time, represented by the model functions $\{f_i\}_i$, and the learning process must be performed separately for each element. Therefore, the concentration of each alloying element is learned independently, and therefore, as many models as alloying elements are needed. This approach is chosen to evaluate whether it can help to overcome typical problems in the quantitative analysis of metals with LIBS, such as matrix effects.

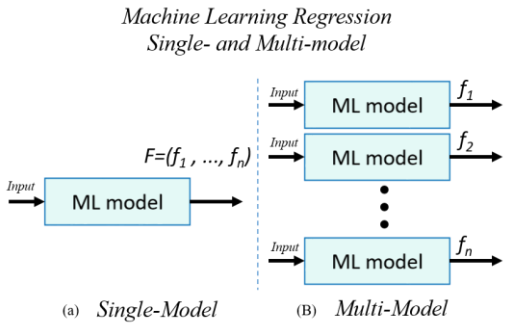

Figure 3.3: Visualisation of the Single-model and Multi-model approaches

3.5. *Deep Learning approach*

The use of convolutional neural networks (CNN) for spectral analysis is steadily increasing [51], [10]. One of the benefits of using Deep Learning is that it allows one to dynamically prioritise difficult tasks. This difficulty is inversely proportional to the performance so that the difficulty changes over time during the training [61], with each task requiring a loss (leading to multiple loss functions). Multiple loss functions were driven by the idea that multiple learning tasks could not be performed by a single function [62]. In this case, learning the concentrations of multiple elements simultaneously and optimising the model for all these tasks could be infeasible with one loss function because the optimisation of different tasks could be fundamentally in conflict or because of limited model capacity. Combining multiple loss functions can also be considered a regularisation, since it restricts the search space for candidate solutions [63].

The approach to loss functions in this article is inspired by loss-conditional training proposed by Dosovitskiy and Djolonga [62]. The idea is to train a single model that covers all coefficients of the loss terms rather than training a model for each set of coefficients. The paper's contribution is to extend the idea of multiple losses to spectral analysis. To the best of the authors' knowledge, this has not been implemented in prior research for spectroscopic regression tasks.

3.5.1. Deep Learning models

A Deep Learning regression method with Single- and Multi-loss functions is proposed to evaluate the effectiveness of the multiple loss functions (Multi-loss), as shown in Figure 3.4. In addition, it is investigated whether the element with the highest concentration influences the regression estimation of the other elements. Therefore, the regression model for estimating the alloying element concentrations was tested with and without including aluminium.

Electronic copy available at: https://ssrn.com/abstract=4284144

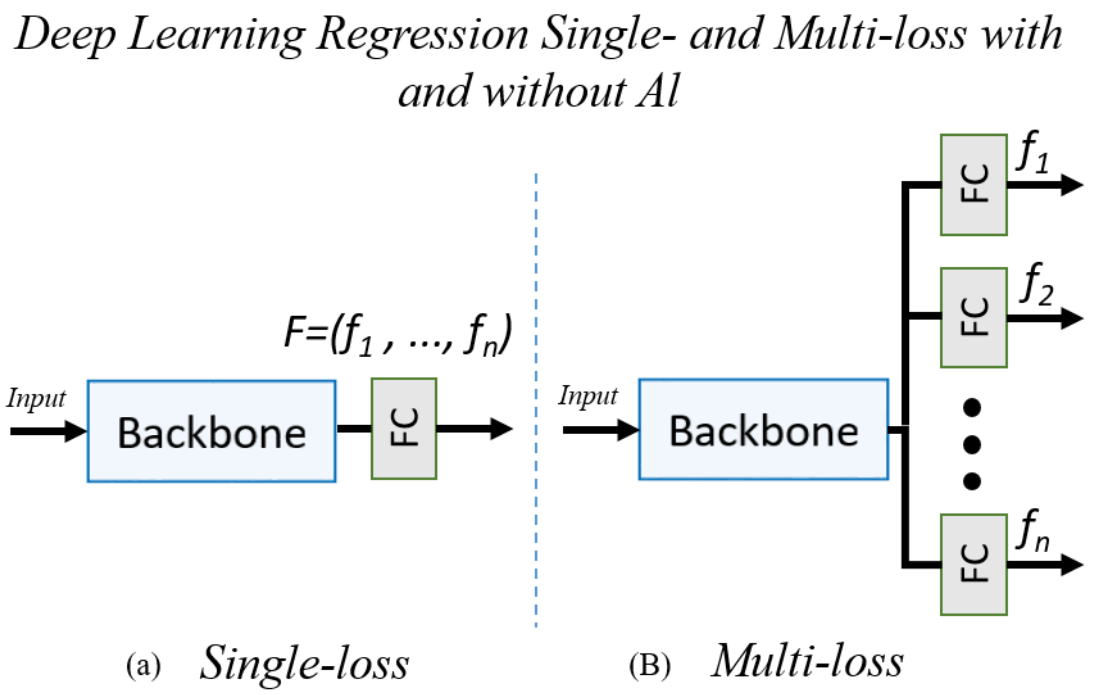

Figure 3.4: Visualisation of the Single-loss and Multi-loss function approach

In Figure 3.4, the Single-loss approach is illustrated on the left, showing the network backbone, which in this case is either a Back Propagation Neural Network (BPNN) or GHOSNET, as proposed in previous work [10], [64], where all the spectrum is fed into the network. The networks were previously used for classification but were adapted by changing the last layer, which is a fully connected layer (FC in Figure 3.4), as well as the networks' activation functions. The backbones are identical in the Single-loss and Multi-loss approach, but in the Multi-loss approach, the last layer is replaced by i fully connected layers, where each one estimates an element model function f_i, i.e. the element concentration, for the i different elements.

The BPNN network backbone has four layers: an input layer (4096, 2048), two hidden layers (1^{st}: (2048,1024), 2^{nd}: (1024: 2048)) with the rectified linear unit (ReLu) as an activation function [65], [10], and a fully connected layer (2048: i) in the Single-loss approach, and i fully connected layers (2048:1) in parallel in the Multi-loss approach, without a linear activation function. GHOSTNET is known to generate more feature maps for cheap operations [64]. In this case, the backbone of the network is maintained, and only the last layer of the network is replaced by fully connected layers, exactly as in the case of the BPNN backbone network.

3.5.2. Training, training parameters, and loss function

Two data augmentation methods were used in this work, inspired by Pytorch's *Audio Feature Augmentation* [10] [66]. The first is *random intensity*, which changes the intensity of the original signal between -30% and +30% of the original signal to mimic a change in the intensity of the spectrum due to surface contamination or irregularities.

The second is *random wavelength masking*, which produces random masks with a width of 0 to 50 nm on the spectrum in the wavelength range between 120 and 404 nm to mimic a spectrum with reduced intensity or saturated peaks. This can occur due to a poor laser-object interaction, which is

Electronic copy available at: https://ssrn.com/abstract=4284144

affected by the angle, distance, and speed of the free-falling object. Data augmentation creates synthetic data from the existing data to increase the number of training epochs and improve the robustness to noise. This step can help reduce overfitting and serve as a regulator to improve the regression performance [67].

The loss function used in both the Single-loss and Multi-loss approach is *Mean Absolute Error* or ℓ_1, which can handle outliers and is more stable than the *Mean Squared Error* or ℓ_2 [68].

Algorithm 1 Multi-loss function

Require:

- elements list $E = \{E_1, \ldots, E_n\}$
- loss function weights vectors $\omega = (\omega_1, \ldots, \omega_n)$ and $w = (w_1, \ldots, w_n)$ ▷ ω weights the first epochs (until n_{steps}) and w weights for the last epochs (from n_{steps})
- number of steps n_{steps}
- training epoch number n_{epoch}
- total number of epochs $\max_{\text{epochs}}$
- index j
- boolean non_element

Ensure:

- loss functions vector $L = (L_{E_1}, \ldots, L_{E_n})$
- total loss ℓ

procedure MULTI-LOSS FUNCTION COMPUTATION
  if non_element = true **then**
    $E \leftarrow \{E_1, \ldots, E_{j-1}, E_{j+1}, \ldots, E_n\}$ ▷ Remove element with index j
    $w \leftarrow (w_1, \ldots, w_{j-1}, w_{j+1}, \ldots, w_n)$
    $\omega \leftarrow (\omega_1, \ldots, \omega_{j-1}, \omega_{j+1}, \ldots, \omega_n)$
  $n \leftarrow$length(E)
  for $1 \leq i \leq \max_{\text{epochs}}$ **do**
    if $n_{\text{epoch}} \leq n_{\text{steps}}$ **then**
      for $1 \leq k \leq n$ **do**
        $L_{E_i} \leftarrow \ell_1$ loss function ▷ $\ell_1 = |\text{predicted} - \text{real value}|$
      $\ell \leftarrow \omega \cdot L = \sum_{i=1}^{n} \omega_i L_{E_i}$
    else
      for $1 \leq k \leq n$ **do**
        $L_{E_i} \leftarrow \ell_1$ loss function
      $\ell \leftarrow w \cdot L = \sum_{i=1}^{n} w_i L_{E_i}$

Figure 3.5: Pseudocode of the Multi-loss function

The pseudocode of the Multi-loss function algorithm is shown in Figure 3.5. The deep learning architecture can be seen as a model for learning the regression model functions $f_1, \ldots, f_n$, where each produces an output. In other words, given n elements $E_1, \ldots, E_n$, the neural network will learn the associated model functions $f_1, \ldots, f_n$, where, for every $1 \leq i \leq n$:

$$f_i: \mathbb{R}^n \rightarrow \mathbb{R} \qquad (3-5)$$

Electronic copy available at: https://ssrn.com/abstract=4284144

The output of each one of these functions is evaluated by a single loss function L_{E_i}, which in this case is the ℓ_1 loss function. The global loss for the stochastic gradient descent algorithm has been computed in previous works as $\ell = L_{E_1} + \cdots + L_{E_n}$. However, it was noticed that the learning could be significantly improved by assigning weights to each one of these sub-loss functions L_{E_i}. Let $\omega = (\omega_1, \dots, \omega_n)$ and $w = (w_1, \dots, w_n)$ be two weight vectors. The first vector, ω, will be assigned to the sub-loss functions in the first epochs (until reaching a predefined limit defined by the input parameter `steps`), while the second vector, w, will be assigned in the last epochs (from the limit defined by the input parameter `steps`):

$$\ell = \begin{cases} \sum_{i=1}^{n} \omega_i L_{E_i} & \text{if epoch} \leq \texttt{steps} \\ \sum_{i=1}^{n} w_i L_{E_i} & \text{if epoch} > \texttt{steps} \end{cases} \quad (3-6)$$

This formula can be rewritten in compact form as $\ell = W \cdot L$, where $(\cdot)$ denotes the scalar product between vectors $L = (L_{E_1}, \dots, L_{E_n})$ and

$$W = \begin{cases} \omega & \texttt{if epoch} \leq \texttt{steps} \\ w & \texttt{if epoch} > \texttt{steps} \end{cases} \quad (3-7)$$

Finally, if one of the n elements $E_1, \dots, E_n$ (for example the base alloy) can be learnt independently or if the concentration of the element does not have to be estimated, it can be omitted, and the remaining elements can still be learnt using the same methodology. If the index j corresponds to the element omitted from the Multi-loss learning, the vectors L, ω, w can be redefined as:

$$L = \left(L_{E_1}, \dots, L_{E_{j-1}}, L_{E_{j+1}}, \dots, L_{E_n}\right) \quad (3-8)$$

$$\omega = \left(\omega_1, \dots, \omega_{j-1}, \omega_{j+1}, \dots, \omega_n\right) \quad (3-9)$$

$$w = \left(w_1, \dots, w_{j-1}, w_{j+1}, \dots, w_n\right) \quad (3-10)$$

Then, the remaining steps of the algorithm are the same as in the original situation.

Lastly, the learning rates for the Single-loss and Multi-loss regression models are set to 0.0001 and 0.001, respectively. In all cases, the Adam Booster algorithm [69] is used together with the gradient descent algorithm as the optimisation method with a zero-weight decay and a learning schedule of [50, 80, 100, 200, 400] with a 0.5 scheduler gamma. Batch sizes of 500 and over 50 epochs are used for the regression sizes, based on previous work [10]. All the models were implemented using Pytorch [66].

4. *Evaluation Metrics*

The performance of all regression methods is evaluated with the same three metrics: the Root-Mean-Square Error (RMSE), the Mean Absolute Error (MAE), and the coefficient of determination (R^2). Equations (4 – 1) to (4 – 3) express how these metrics are defined. In these equations, y_i denotes the ground truth values for the element concentrations, $\hat{y}_i$ denotes the predicted element concentration values, $\bar{y}$ denotes the average ground truth values, and N the number of samples. The RMSE is thus the standard deviation of the residuals (prediction errors), the MAE is the arithmetic average of the absolute errors on the predictions, regardless of the direction of over- or under-prediction, and the R^2 value is the proportion of variation in the dependent variable that is predictable from the independent variable and therefore represents how well the model fits the dependent variables.

$$\text{RMSE} = \sqrt{\frac{(y_i - \hat{y}_i)^2}{N}} \quad (4-1)$$

Electronic copy available at: https://ssrn.com/abstract=4284144

$$\mathrm{MAE} = \frac{1}{N}\sum_{i}|y_i - \hat{y}_i| \qquad (4-2)$$

$$R^2 = \frac{\sum_i (y_i - \hat{y}_i)^2}{\sum_i (y_i - \bar{y}_i)^2} \qquad (4-3)$$

5. *Results and Discussion*

This chapter presents the results of the different regression strategies. First, the results are reported for the tested traditional regression methods. Afterwards, the results are demonstrated for the developed Deep learning approach. The traditional regression methods evaluated in this article are univariate regression and two Machine Learning methods: Random Forest (RF) and Logistic Regression (LR).

5.1. *Univariate regression*

Table 5.1 shows the performance of the linear univariate regression method for the Reference Sample set and Scrap Sample set in terms of RMSE, MAE, and R^2 values. The table only contains the predictions for the alloying elements and not the base element aluminium because aluminium is used as the reference element in the univariate regression, as explained in the *Methods* section. While the performance of the univariate method is relatively good for some elements in the Reference Sample set, the method has a poor performance for most elements in the Scrap Sample set. Regarding the predictions for the Scrap Sample pieces, moderate results are achieved for Si, with an RMSE, MAE, and R^2 value of 0.22 wt.%, 0.10 wt.%, and 0.66, respectively.

Considering that the concentration of Si is above 10 wt.% for most cast alloy pieces and ranges up to almost 20 wt.% for some, as illustrated in Figure 3.2, the MAE of 0.10 wt.% actually corresponds to a low relative error in comparison to most other elements, whose concentrations are typically around or below 1 wt.%. For Fe, Mn, and Zn, the R^2 value is especially poor, indicating the difficulty of fitting a linear function on the data points for these elements. In general, the MAE is in the order of magnitude of 0.1 wt.% or 1000 ppm for most elements. Therefore, the linear univariate regression method does not predict the alloying elements' concentrations accurately enough for the intended sorting tasks.

Table 5.1: Regression performance of the univariate method in terms of RMSE, MAE, and R^2

	Univariate regression					
	RMSE (wt.%)		**MAE (wt.%)**		**R^2 (-)**	
	References	**Scrap**	**References**	**Scrap**	**References**	**Scrap**
Si	0.16	0.22	0.12	0.10	0.89	0.66
Fe	0.02	0.11	0.02	0.08	0.51	0.09
Cu	0.10	0.09	0.06	0.07	0.94	0.59
Mn	0.09	0.11	0.06	0.08	0.83	0.03
Mg	0.11	0.37	0.08	0.32	0.76	0.72
Zn	0.04	0.05	0.02	0.02	0.44	0.06

Electronic copy available at: https://ssrn.com/abstract=4284144

5.2. *Machine Learning*

The regression performance of the Machine Learning models is shown in Table 5.2 and Table 5.3 for the Reference Sample pieces and the Scrap Sample pieces, respectively. The results of four experiments are shown in Table 5.2, corresponding to the different combinations of the Machine Learning model (Random Forest and Logistic Regression) and the Single-/Multi-Model approach. The best score among the four methods is indicated in bold for every metric and element. Random Forest Regression outperforms Logistic Regression for all three metrics (RMSE, MAE, and R^2) for all elements.

The comparison between the Single-Model and the Multi-Model approach is not as straightforward. For Si, Fe, and Mg, the Single-Model approach (using RF) yields the best results, while the Multi-Model approach yields the best results for Cu and Zn. For Al and Mn, the metrics do not concur on the best method. The best Machine Learning method results for each element in terms of R^2 value range from 0.93 to 1.00 for all elements except Fe, which indicates that the Machine Learning models can fit the spectral data for the Reference Sample pieces very well. However, some pieces still affect the overall RMSE and MAE. This corresponds very well with the conclusions of previous work in LIBS, mentioned in the *Introduction*, that has addressed the regression issue on clean certified aluminium samples.

Table 5.2: Regression performance in terms of RMSE, MAE, and R^2 for all combinations of Machine Learning models (Random Forest and Logistic Regression) and Single-/Multi-Model strategies for the Reference Sample set

		Machine Learning					
		RMSE (wt.%)		**MAE (wt.%)**		**R^2 (-)**	
		RF	**LR**	**RF**	**LR**	**RF**	**LR**
Al	Single-Model	0.93	1.91	**0.46**	1.53	**0.97**	0.85
	Multi-Model	**0.89**	1.42	0.51	1.13	**0.97**	0.92
Si	Single-Model	**0.70**	1.37	**0.32**	1.05	**0.97**	0.89
	Multi-Model	0.80	1.11	0.37	0.87	0.96	0.93
Fe	Single-Model	**0.09**	0.16	**0.04**	0.11	**0.85**	0.56
	Multi-Model	0.11	0.12	0.05	0.09	0.80	0.76
Cu	Single-Model	0.11	0.31	0.04	0.21	0.99	0.92
	Multi-Model	**0.07**	0.20	**0.03**	0.15	**1.00**	0.97
Mn	Single-Model	**0.07**	0.11	0.04	0.08	**0.96**	0.88
	Multi-Model	0.08	0.10	**0.03**	0.07	0.93	0.91
Mg	Single-Model	**0.22**	0.51	**0.08**	0.26	**0.95**	0.76
	Multi-Model	0.25	0.38	0.09	0.28	0.94	0.87
Zn	Single-Model	0.56	0.92	0.15	0.64	0.88	0.67
	Multi-Model	**0.43**	0.66	**0.14**	0.51	**0.93**	0.83

For the pieces in the Scrap Sample set, the Single-Model approach using Random Forest Regression yields the best results for Al, Si, Cu, Mg, and Zn. The Multi-Model approach using RF performs best for Mn. The overall performance in predicting Fe concentrations is low for all methods. As for the Reference Sample set, the best score for every metric and element is in bold in Table 5.3. Overall, the results are worse for the Scrap Sample set than for the Reference Sample set, as should be expected. The surface condition of the scrap pieces clearly impacts the quality of the LIBS spectra for quantitative analysis.

Nevertheless, the R^2 values of the best performing Machine Learning method for each element range from 0.64 to 0.89 for the Scrap Sample pieces. This is a significant improvement with respect to the R^2 values achieved with the univariate regression method, which range from just 0.03 to 0.72. The

Electronic copy available at: https://ssrn.com/abstract=4284144

higher score for this metric indicates that the Machine Learning models better fit the data. However, the RMSE and MAE are still an order of magnitude too high for the intended sorting tasks. While the models better fit the data, outliers still heavily impact the overall accuracy of the predictions. This conclusion highlights the need for a method that goes beyond the state-of-the-art in LIBS regression methods to achieve a system with sufficient accuracy to sort aluminium scrap based on the prediction of alloying element concentrations.

Table 5.3: Regression performance in terms of RMSE, MAE, and R^2 for all combinations of Machine Learning models (Random Forest and Logistic Regression) and Single-/Multi-Model strategies for the Scrap Sample set

		Machine Learning					
		RMSE (wt.%)		**MAE (wt.%)**		**R^2 (-)**	
		RF	**LR**	**RF**	**LR**	**RF**	**LR**
Al	Single-Model	**1.98**	3.00	**1.19**	2.36	**0.89**	0.74
	Multi-Model	4.57	5.85	1.81	2.57	0.45	0.09
Si	Single-Model	**1.62**	2.59	**0.83**	1.89	**0.88**	0.69
	Multi-Model	1.74	3.52	0.86	1.84	0.86	0.42
Fe	Single-Model	0.28	**0.24**	**0.17**	0.18	0.21	**0.43**
	Multi-Model	3.81	1.70	0.71	1.04	0	0
Cu	Single-Model	**0.49**	0.64	**0.25**	0.39	**0.78**	0.62
	Multi-Model	0.58	0.74	0.29	0.74	0.75	0.59
Mn	Single-Model	0.32	0.33	0.19	0.20	0.08	0.04
	Multi-Model	**0.18**	0.31	**0.11**	0.18	**0.69**	0.04
Mg	Single-Model	**0.49**	0.56	**0.27**	0.39	**0.69**	0.59
	Multi-Model	0.83	1.92	0.33	0.74	0.22	0
Zn	Single-Model	**0.35**	0.55	**0.16**	0.31	**0.64**	0.13
	Multi-Model	0.50	0.74	0.23	0.48	0.42	0

5.3. *Deep Learning approach*

The regression performance of the Deep Learning methods are shown in Table 5.4 and Table 5.5 for the Reference Sample set and Scrap Sample set, respectively. Both tables show the scores of the three metrics (RMSE, MAE, and R^2) that are used to evaluate the performance of the eight Deep Learning experiments for all elements. For each element and metric, the combination of the backbone model (BPNN or Ghostnet), loss function approach (Single- or Multi-loss), and base alloy strategy (included or not) that has the best score is indicated in bold. If multiple combinations have the same score, all are in bold. In the Reference Sample set, the concentration of Al is best predicted by Ghostnet with the Multi-loss approach. BPNN with the Multi-loss approach without excluding aluminium from the learning yields the lowest RMSE and MAE for all other elements. For Fe and Cu, the same RMSE and MAE can be achieved using Ghostnet, while the Single-loss approach for Mg leads to the same RMSE and MAE. The highest R^2 values are achieved for all elements when the base alloy aluminium is excluded from the learning. For Si, Cu, and Zn, Ghostnet with the Multi-loss approach yields the highest R^2 values, while for Fe, Mn, and Mg, the highest R^2 values are achieved with BPNN and the Single-loss approach.

So, the Multi-loss approach leads to the smallest RMSE and MAE for all elements. The RMSE and MAE are up to 0.12 wt.% and 0.10 wt.% lower, respectively, with respect to the Single-loss approach. Adopting the Multi-loss approach also increases the coefficient of determination for all elements except Fe, Mn, and Mg, making the models fit better to the spectral data. BPNN yields the best performance in terms of RMSE and MAE, while for the R^2 value, the best model depends on the element. Including the base alloy in the learning reduces the RMSE and MAE for all elements but not necessarily the R^2 values.

Electronic copy available at: https://ssrn.com/abstract=4284144

Table 5.4: Regression performance in terms of RMSE, MAE, and R^2 for all combinations of backbone models (BPNN and Ghostnet), loss function approaches (Single-loss and multi-loss) and base alloy strategies (including and excluding aluminium) for the Reference Sample set

		BPNN						**GHOSTNET**					
		RMSE (wt.%)		**MAE (wt.%)**		**R^2 (-)**		**RMSE (wt.%)**		**MAE (wt.%)**		**R^2 (-)**	
		With Al	With out Al	With Al	With out Al	With Al	With out Al	With Al	With out Al	With Al	With out Al	With Al	With out Al
Al	S-Loss	0.15		0.12		0.33		0.04		0.03		0.72	
	M-Loss	0.03		**0.02**		0.93		**0.02**		**0.02**		**0.94**	
Si	S-Loss	0.04	0.19	0.03	0.11	0.74	0.91	0.04	0.54	0.04	0.33	0.51	0.00
	M-Loss	**0.01**	0.17	**0.01**	0.09	0.95	0.93	0.02	0.11	**0.01**	0.06	0.95	**0.98**
Fe	S-Loss	**0.00**	0.01	**0.00**	0.01	0.43	**0.78**	0.01	0.03	0.01	0.03	0.31	0.21
	M-Loss	**0.00**	0.02	**0.00**	0.01	0.62	0.69	**0.00**	0.01	**0.00**	0.01	0.61	0.77
Cu	S-Loss	**0.01**	0.06	0.01	0.03	0.58	0.90	**0.01**	0.12	0.01	0.06	0.61	0.22
	M-Loss	**0.01**	0.09	**0.00**	0.04	0.78	0.69	**0.01**	0.04	**0.00**	0.02	0.83	**0.94**
Mn	S-Loss	0.01	0.02	0.01	0.02	0.29	**0.89**	0.01	0.03	**0.00**	0.02	0.09	0.02
	M-Loss	**0.00**	0.02	**0.00**	0.01	0.74	0.77	0.01	0.02	**0.00**	0.01	0.73	0.79
Mg	S-Loss	**0.01**	0.04	**0.00**	0.02	0.89	**0.92**	**0.01**	0.13	0.01	0.08	0.39	0.23
	M-Loss	**0.01**	0.05	**0.00**	0.02	**0.92**	0.91	**0.01**	0.06	**0.00**	0.03	0.84	0.82
Zn	S-Loss	0.02	0.14	**0.01**	0.05	0.52	0.78	0.02	0.18	**0.01**	0.07	0.05	0.00
	M-Loss	**0.01**	0.14	**0.01**	0.05	0.74	0.77	**0.01**	0.07	**0.01**	0.03	0.84	**0.96**

In the Scrap Sample set, the concentrations of Al are best predicted by BPNN with the Multi-loss approach. For Si, Cu, and Zn, BPNN with the Multi-loss approach without excluding the base alloy aluminium yields the best results over all metrics. However, the same performance is achieved for Zn with the Single-loss approach. For Fe, Mn, and Mg, BPNN with the Multi-loss approach without excluding the base alloy also yields the lowest RMSE and MAE, but for these elements, the R^2 value is higher when the base alloy is excluded. BPNN consistently has the best performance for the Scrap Sample set, although the results are often the same or similar for Ghostnet.

There is no case, in any of the metrics, where the Single-loss approach outperforms the Multi-loss approach. Excluding the base alloy from the learning only improves the R^2 values of Fe, Mn, and Mg. So, adopting the Multi-loss approach, with one loss function for each element, has proven its significant value for the regression performance, as it improves the scores for all metrics in both the Reference and Scrap Sample set. The effect of excluding Al from the learning is mostly small and not always positive, but demonstrating this effect is also considered valuable.

Electronic copy available at: https://ssrn.com/abstract=4284144

Table 5.5: Regression performance in terms of RMSE, MAE, and R^2 for all combinations of backbone models (BPNN and Ghostnet), loss function approaches (Single-loss and Multi-loss) and base alloy strategies (including and excluding aluminium) for the Scrap Sample set

		BPNN						**GHOSTNET**					
		RMSE (wt.%)		**MAE (wt.%)**		**R^2 (-)**		**RMSE (wt.%)**		**MAE (wt.%)**		**R^2 (-)**	
		With Al	With out Al	With Al	With out Al	With Al	With out Al	With Al	With out Al	With Al	With out Al	With Al	With out Al
Al	S-Loss	0.13		0.11		0.04		0.07		0.06		0.45	
	M-Loss	**0.03**		**0.02**		**0.93**		**0.03**		**0.02**		0.87	
Si	S-Loss	0.03	0.22	0.02	0.13	0.86	0.90	0.05	0.30	0.03	0.17	0.22	0.80
	M-Loss	**0.02**	0.19	**0.01**	0.09	**0.94**	0.92	**0.02**	0.16	0.02	0.08	0.88	**0.94**
Fe	S-Loss	0.01	0.04	0.01	0.02	0.53	**0.58**	0.02	0.03	0.02	0.02	0.22	0.57
	M-Loss	**0.00**	0.03	**0.00**	0.02	0.57	**0.58**	**0.00**	0.03	**0.00**	0.02	0.57	0.57
Cu	S-Loss	**0.01**	0.07	0.01	0.04	0.78	0.80	**0.01**	0.08	0.01	0.04	0.08	0.73
	M-Loss	**0.01**	0.07	**0.00**	0.03	**0.82**	0.81	**0.01**	0.07	0.01	0.03	0.77	0.81
Mn	S-Loss	0.01	0.03	**0.00**	0.01	**0.31**	**0.31**	0.02	0.03	0.02	0.01	0.10	0.18
	M-Loss	**0.00**	0.03	**0.00**	0.01	0.27	**0.31**	**0.00**	0.03	**0.00**	0.01	0.24	0.20
Mg	S-Loss	**0.01**	0.06	**0.00**	0.03	0.80	0.84	**0.01**	0.09	0.01	0.05	0.20	0.43
	M-Loss	**0.01**	0.05	**0.00**	0.03	0.79	**0.85**	**0.01**	0.10	0.01	0.05	0.37	0.29
Zn	S-Loss	**0.01**	0.10	**0.00**	0.03	**0.30**	0.28	0.04	0.10	0.04	0.03	0.04	0.25
	M-Loss	**0.01**	0.10	**0.00**	0.03	**0.30**	0.28	**0.01**	0.10	**0.00**	0.03	0.28	0.24

6. *Implications for sorting*

The presented regression methodology has been developed with the intent of implementing a similar method in an industrial sorting process. The benefit of an accurate regression method is that the sorting decision (the assignment of a scrap piece to one of the output classes) can be made with a decision tree based on the estimated alloying element concentrations. When the needs of the sorter change and the definition of the output classes has to be adapted, the regression approach requires only the adaptation of the decision tree, and the entire Deep Learning model does not have to be retrained for the new classes. This is a considerable improvement with respect to a sorting strategy that relies directly on a Deep Learning classifier, as presented in the authors' earlier work [10], where the system has to be retrained for every change in the desired output fractions. This advantage is critical to make a LIBS-based sorting system effective in an industrial sorting context.

The authors have also refrained from making the regression method tailored to the specific issue of sorting post-consumer aluminium scrap. The intent was to make a generic method to estimate alloying element concentrations and trace amounts that could also be used for other materials. Therefore, the regression method does not comprise a feature extraction step and does not rely on intensities at specific wavelengths that need to be manually selected, as is the case for the univariate regression method. Furthermore, the authors have made significant effort to make the method ready for industry regarding the computational cost and the time needed to process the spectral data. For the best performing Deep Learning regression models, the time it takes to perform the pre-processing and estimate the alloying element concentrations is just between 1 and 3 ms for up to 200 spectra simultaneously. Therefore, the quantitative analysis can be performed in time for an industrial sorting process, even at high throughputs. The Deep Learning system is also relatively easy to train, and measures such as data augmentation have been taken to avoid overfitting.

Finally, what distinguishes this method most from results reported in previous research, is the ability to achieve high accuracy in the prediction of alloying element concentrations, even for post-consumer scrap pieces with significant surface contamination. For Cu, Mn, and Zn, the best performing Deep Learning models achieve an RMSE and MAE below 0.01 wt.% or 100 ppm. To the best of the authors' knowledge, this is unprecedented and, at the same time, necessary to enable wrought-to-wrought recycling. Remelters of secondary wrought alloys typically demand scrap for which the concentrations of Cu, Mn, and Zn are below a threshold of just around 0.05 wt.% or 500 ppm, which is nowadays almost exclusively achievable by diluting with manufacturing scrap or primary aluminium

Electronic copy available at: https://ssrn.com/abstract=4284144

[3] [9]. Also, for Al, Si, and Mg, which typically have a higher concentration than Cu, Mn, and Zn, and for which the thresholds set by remelters are less stringent, the RMSE is limited to 0.02 wt.%, 0.02 wt.%, and 0.01 wt.%, respectively.

Based on the presented results and these considerations, the authors believe that the presented Deep Learning regression method is a significant contribution to the goal of European Aluminium to implement LIBS-based sorting systems by the end of the decade, as well as to the field of quantitative LIBS analysis in general.

7. *Conclusion and Future Work*

This paper presents a Deep Learning regression method for estimating alloying element concentrations for aluminium reference and post-consumer scrap pieces. While the regression method is only evaluated for aluminium material, it is developed to be applicable for other metals as well. One of the key contributions is the use of multiple loss functions for the multi-task learning problem of estimating the concentrations of multiple alloying elements. Adopting a Multi-loss approach, with one loss function for each element, has a significant added value for the regression performance. It improves the results for all performance metrics in the Scrap Sample set, and the same is true for the Reference Sample set, except for the coefficient of determination of Fe, Mn, and Mg. In addition, the proposed methodology considers the learning prioritisation problem to prevent that learning the concentration of the base alloy is prioritised over the alloying elements. Although the effect of excluding Al from the learning is small and not always positive for the performance, demonstrating this effect is also considered valuable. Since the RMSE on the prediction is just 0.02 wt.% for Al and Si, and not more than 0.01 wt.% for Fe, Cu, Mn, Mg, and Zn, the best performing Deep Learning models show promise for the future of LIBS in metal sorting applications.

Future research will investigate methods to optimise the proposed regression model's hyperparameters to further improve the learning with the Multi-loss approach. Since the weight vectors ω and w can be considered as two hyperparameters of the proposed model, they can also be learnt during the training process. Therefore, grid-search and (nested) cross-validation will be used for hyperparameter tuning. In addition, the integration of the proposed regression method with a computer vision system with RGB and depth cameras will be investigated. This will allow to overcome the LIBS system's limitations on heavily contaminated material, e.g. pieces with painted or heavily oxidised surfaces.

Finally, future research will investigate optimal approaches to integrate the developed regression systems into a real-time sorting system for post-consumer aluminium scrap. Such a sorting system should enable more wrought-to-wrought recycling and reduce quality losses that are today common in aluminium scrap recycling. That way, more value can be recovered from post-consumer aluminium scrap, and the recycling industry can move to a more circular and sustainable way of managing this material.

ACKNOWLEDGMENTS

Special thanks to Alexander Eckert and to Redwave, SPECTRAL Industries, RISE, and Swerim AB for developing the LIBS system and providing constant feedback throughout the project. This activity has received funding from the European Institute of Innovation and Technology (EIT), a body of the European Union, under the Horizon 2020, the EU Framework Programmes for Research and Innovation (project name: AUtomatic SOrting of mixed scrap Metals (AUSOM project – www.ausomproject.eu), project number: 19294). The AUSOM project consists of a consortium of seven expert organizations (Galloo, LTU Business, Spectral Industries, Swerim AB, Redwave, RISE, and KU Leuven).

Electronic copy available at: https://ssrn.com/abstract=4284144

REFERENCES

[1] European Aluminium Association, 'Circular aluminium action plan - A strategy for achieving aluminium's full potential for circular economy by 2030', European Aluminium Association, Brussels, Belgium, 2019. [Online]. Available: https://www.european-aluminium.eu/media/2906/european-aluminium-circular-aluminium-action-plan.pdf

[2] Aluminium Innovation Hub, 'Mapping key objectives and R&D challenges along the aluminium value chain', European Aluminium Association, Brussels, Belgium, May 2016. [Online]. Available: https://www.european-aluminium.eu/media/3313/european-aluminum-innovation-hub-mapping-report-v1.pdf

[3] S. Van den Eynde, E. Bracquené, D. Diaz-Romero, B. Engelen, J. R. Duflou, and J. R. Peeters, 'Forecasting global aluminium flows to demonstrate the need for improved sorting and recycling methods', *Waste Management*, vol. 137, pp. 231–240, Jan. 2022, doi: 10.1016/j.wasman.2021.11.019.

[4] D. Paraskevas, K. Kellens, W. Dewulf, and J. R. Duflou, 'Environmental modelling of aluminium recycling: a Life Cycle Assessment tool for sustainable metal management', *Journal of Cleaner Production*, vol. 105, pp. 357–370, Oct. 2015, doi: 10.1016/j.jclepro.2014.09.102.

[5] R. Modaresi, A. N. Løvik, and D. B. Müller, 'Component- and Alloy-Specific Modeling for Evaluating Aluminum Recycling Strategies for Vehicles', *JOM*, vol. 66, no. 11, Art. no. 11, Nov. 2014, doi: 10.1007/s11837-014-0900-8.

[6] H. Buchner, D. Laner, H. Rechberger, and J. Fellner, 'Potential recycling constraints due to future supply and demand of wrought and cast Al scrap - A closed system perspective on Austria', *Resources, conservation and recycling*, vol. 122, pp. 135–142, Jul. 2017, doi: 10.1016/j.resconrec.2017.01.014.

[7] L. Zhan *et al.*, 'A rapid classification method of aluminum alloy based on laser-induced breakdown spectroscopy and random forest algorithm', *Plasma Science and Technology*, vol. 21, 2019, doi: 10.1088/2058-6272/aaf7bf.

[8] E. Harefa and W. Zhou, 'Laser-Induced Breakdown Spectroscopy Combined with Nonlinear Manifold Learning for Improvement Aluminum Alloy Classification Accuracy', *Sensors*, vol. 22, no. 9, Apr. 2022, doi: 10.3390/s22093129.

[9] S. Van den Eynde, D. J. Díaz-Romero, B. Engelen, I. Zaplana, and J. Peeters, 'Assessing the efficiency of Laser-Induced Breakdown Spectroscopy (LIBS) based sorting of post-consumer aluminium scrap', in *Procedia CIRP*, Leuven, Belgium, 2022, vol. 105, pp. 278–283. doi: doi: 10.1016/j.procir.2022.02.046.

[10] D. J. Díaz-Romero *et al.*, 'Real-time classification of aluminum metal scrap with laser-induced breakdown spectroscopy using deep and other machine learning approaches', *Spectrochimica Acta Part B: Atomic Spectroscopy*, vol. 196, p. 106519, Oct. 2022, doi: https://doi.org/10.1016/j.sab.2022.106519.

[11] B. Campanella *et al.*, 'Classification of wrought aluminum alloys by Artificial Neural Networks evaluation of Laser Induced Breakdown Spectroscopy spectra from aluminum scrap samples', *Spectrochimica Acta Part B: Atomic Spectroscopy*, vol. 134, pp. 52–57, 2017, doi: 10.1016/j.sab.2017.06.003.

[12] P. Werheit, C. Fricke-Begemann, M. Gesing, and R. Noll, 'Fast single piece identification with a 3D scanning LIBS for aluminium cast and wrought alloys recycling', *Journal of Analytical Atomic Spectrometry*, vol. 26, no. 11, pp. 2166–2174, 2011, doi: 10.1039/C1JA10096C.

[13] S. Legnaioli *et al.*, 'Industrial applications of laser-induced breakdown spectroscopy: a review', *Analytical Methods*, vol. 12, pp. 1014–1029, Feb. 2020, doi: 10.1039/C9AY02728A.

[14] SECOPTA analystics GmbH, 'Recycling of aluminum: Separation into close specification categories'. [Online]. Available: https://www.secopta.com/applications/recycling

[15] B. Noharet *et al.*, 'A compact LIBS system for industrial applications', in *Photonic Instrumentation Engineering II*, San Francisco, California, USA, Mar. 2015, vol. 9369. doi: 10.1117/12.2075336.

Electronic copy available at: https://ssrn.com/abstract=4284144

[16] J. Gurell, A. Bengston, M. Falkenström, and B. A. M. Hansson, 'Laser induced breakdown spectroscopy for fast elemental analysis and sorting of metallic scrap pieces using certified reference materials', *Spectrochimica Acta Part B: Atomic Spectroscopy*, vol. 74–75, pp. 46–50, 2012, doi: 10.1016/j.sab.2012.06.013.
[17] M. Kuzuya, 'A Sorting System for Aluminum Alloy Scrap Based on Laser-Induced Breakdown Spectroscopy', *Science Journal of Analytical Chemistry*, vol. 7, no. 3, pp. 65–71, May 2019, doi: 10.11648/j.sjac.20190703.11.
[18] H. Hegazy, E. A. Abdel-Wahab, F. M. Abdel-Rahim, S. H. Allam, and A. M. A. Nossair, 'Laser-induced breakdown spectroscopy: technique, new features, and detection limits of trace elements in Al base alloy', *Applied Physics B*, vol. 115, pp. 173–183, 2014, doi: 10.1007/s00340-013-5589-9.
[19] Z. Xu *et al.*, 'Laser-ablation dependence of fiber-laser-based laser-induced breakdown spectroscopy for determining Cu, Mg, and Mn elements in aluminum alloys', *Journal of Analytical Atomic Spectrometry*, vol. 36, pp. 2501–2508, Sep. 2021, doi: 10.1039/d1ja00188d.
[20] H. Li, M. Liu, Z. Chen, and R. Li, 'Quantitative analysis of impurities in aluminum alloys by laser-induced breakdown spectroscopy without internal calibration', *Transactions of Nonferrous Metals Society of China*, vol. 18, no. 1, pp. 222–226, Feb. 2008, doi: 10.1016/S1003-6326(08)60040-0.
[21] S. Zivkovic, J. Savovic, M. Trtica, J. Mutic, and M. Momcilovic, 'Elemental analysis of aluminum alloys by Laser Induced Breakdown Spectroscopy based on TEA CO2 laser', *Journal of Alloys and Compounds*, vol. 700, pp. 175–184, Apr. 2017, doi: 10.1016/j.jallcom.2017.01.060.
[22] B. N. Bennett, M. Z. Martin, D. N. Leonard, and E. Garlea, 'Calibration curves for commercial copper and aluminum alloys using handheld laser-induced breakdown spectroscopy', *Applied Physics B*, vol. 124, Feb. 2018, doi: 10.1007/s00340-018-6909-x.
[23] J. Wu *et al.*, 'Plasma characteristics and element analysis of steels from a nuclear power plant based on fiber-optic laser-induced breakdown spectroscopy', *Journal of Physics D: Applied Physics*, vol. 52, 2019, doi: 10.1088/1361-6463/aae7b4.
[24] K. G. Myhre, M. J. Mehta, M. Z. Martin, and M. Du, 'Laser Induced Breakdown Spectroscopy analysis of europium and samarium in aluminum oxide', *Spectrochimica Acta Part B: Atomic Spectroscopy*, vol. 149, pp. 30–34, Nov. 2018, doi: 10.1016/j.sab.2018.07.014.
[25] S. H. Gudmundsson, J. Matthiasson, B. M. Björnsson, H. Gudmundsson, and K. Leosson, 'Quantitative in-situ analysis of impurity elements in primary aluminum processing using laser-induced breakdown spectroscopy', *Spectrochimica Acta Part B: Atomic Spectroscopy*, vol. 158, Aug. 2019, doi: 10.1016/j.sab.2019.105646.
[26] W. Wang, L. Sun, P. Zhang, T. Chen, L. Zheng, and L. Qi, 'Study of matrix effects in laser-induced breakdown spectroscopy by laser defocus and temporal resolution', *Journal of Analytical Atomic Spectrometry*, vol. 36, pp. 1977–1985, 2021, doi: 10.1039/d1ja00179e.
[27] Y. M. Guo *et al.*, 'Accuracy improvement of iron ore analysis using laser-induced breakdown spectroscopy with a hybrid sparse partial least squares and least-squares support vector machine model', *Journal of Analytical Atomic Spectrometry*, vol. 33, pp. 1330–1335, 2018, doi: 10.1039/c8ja00119g.
[28] C. Yan, J. Qi, J. Ma, H. Tang, T. Zhang, and H. Li, 'Determination of carbon and sulfur content in coal by laser induced breakdown spectroscopy combined with kernel-based extreme learning machine', *Chemometrics and Intelligent Laboratory Systems*, vol. 167, pp. 226–231, 2017, doi: 10.1016/j.chemolab.2017.06.006.
[29] T. Chen, L. Zhang, L. Huang, M. Liu, J. Chen, and M. Yao, 'Quantitative analysis of chromium in pork by PSO-SVM chemometrics based on laser induced breakdown spectroscopy', *Journal of Analytical Atomic Spectrometry*, vol. 34, pp. 884–890, 2019, doi: 10.1039/c8ja00392k.
[30] J. El Haddad *et al.*, 'Application of a series of artificial neural networks to on-site quantitative analysis of lead into real soil samples by laser induced breakdown spectroscopy', *Spectrochimica Acta Part B: Atomic Spectroscopy*, vol. 97, pp. 57–64, Jul. 2014, doi: 10.1016/j.sab.2014.04.014.

Electronic copy available at: https://ssrn.com/abstract=4284144

[31] M. Darby Dyar *et al.*, 'Comparison of univariate and multivariate models for prediction of major and minor elements from laser-induced breakdown spectra with and without masking', *Spectrochimica Acta Part B: Atomic Spectroscopy*, vol. 123, pp. 93–104, 2016, doi: 10.1016/j.sab.2016.07.010.
[32] H. Lu, X. Hu, L. Ma, M. Li, and B. Cao, 'Measurement of the molecular ratio of Aluminum electrolytes using laser-induced breakdown spectroscopy', *Spectrochimica Acta Part B: Atomic Spectroscopy*, vol. 164, Feb. 2020, doi: 10.1016/j.sab.2019.105753.
[33] X. Li, H. Lu, J. Yang, and F. Chang, 'Semi-supervised LIBS quantitative analysis method based on co-training regression model with selection of effective unlabeled samples', *Plasma Science and Technology*, vol. 21, 2019, doi: 10.1088/2058-6272/aaee14.
[34] E. Kim, Y. Kim, E. Srivastava, S. Shin, S. Jeong, and E. Hwang, 'Soft classification scheme with pre-cluster-based regression for identification of same-base alloys using laser-induced breakdown spectroscopy', *Chemometrics and Intelligent Laboratory Systems*, vol. 203, Aug. 2020, doi: 10.1016/j.chemolab.2020.104072.
[35] S. M. Clegg *et al.*, 'Recalibration of the Mars Science Laboratory ChemCam instrument with an expanded geochemical database', *Spectrochimica Acta Part B: Atomic Spectroscopy*, vol. 129, pp. 64–85, 2017, doi: 10.1016/j.sab.2016.12.003.
[36] Q. Shi, G. Niu, Q. Lin, T. Xu, F. Li, and Y. Duan, 'Quantitative analysis of sedimentary rocks using laser-induced breakdown spectroscopy: comparison of support vector regression and partial least squares regression chemometric methods', *Journal of Analytical Atomic Spectrometry*, vol. 30, pp. 2384–2393, 2015, doi: 10.1039/C5JA00255A.
[37] T. F. Boucher *et al.*, 'A study of machine learning regression methods for major elemental analysis of rocks using laser-induced breakdown spectroscopy', *Spectrochimica Acta Part B: Atomic Spectroscopy*, vol. 107, pp. 1–10, May 2015, doi: 10.1016/j.sab.2015.02.003.
[38] C. R. Ytsma, C. A. Knudson, M. Darby Dyar, A. C. McAdam, D. D. Michaud, and L. M. Rollosson, 'Accuracies and detection limits of major, minor, and trace element quantification in rocks by portable laser-induced breakdown spectroscopy', *Spectrochimica Acta Part B: Atomic Spectroscopy*, vol. 171, Sep. 2020, doi: 10.1016/j.sab.2020.105946.
[39] K. Rifai *et al.*, 'Rapid analysis of phosphate slurries and pressed pellets using laser-induced breakdown spectroscopy', *Spectrochimica Acta Part B: Atomic Spectroscopy*, vol. 163, Jan. 2020, doi: 10.1016/j.sab.2019.105735.
[40] N. Ahmed *et al.*, 'Machine learning-based calibration LIBS analysis of aluminium-based alloys', *The European Journal Plus*, vol. 137, May 2022, doi: 10.1140/epjp/s13360-022-02892-4.
[41] P. Inakollu, T. Philip, A. K. Rai, F.-Y. Yueh, and J. P. Singh, 'A comparative study of laser induced breakdown spectroscopy analysis for element concentrations in aluminum alloy using artificial neural networks and calibration methods', *Spectrochimica Acta Part B: Atomic Spectroscopy*, vol. 64, no. 1, pp. 99–104, Jan. 2009, doi: 10.1016/j.sab.2008.11.001.
[42] A. H. Farhadian and S. S. M. Fard, 'Quantitative Analysis and Identification Improvement in Laser-Induced Breakdown Spectroscopy by Self-Absorption Correction and Artificial Neural Network', *IEEE Transactions on Plasma Science*, vol. 49, no. 12, pp. 3853–3859, Dec. 2021, doi: 10.1109/TPS.2021.3123434.
[43] Y. Dai, C. Song, X. Gao, A. Chen, Z. Hao, and J. Lin, 'Quantitative determination of Al–Cu–Mg–Fe–Ni aluminum alloy using laser-induced breakdown spectroscopy combined with LASSO–LSSVM regression', *Journal of Analytical Atomic Spectrometry*, vol. 63, pp. 1629–1634, 2021, doi: 10.1002/mop.32810.
[44] F. R. Doucet, T. F. Belliveau, J.-L. Fortier, and J. Hubert, 'Use of chemometrics and laser-induced breakdown spectroscopy for quantitative analysis of major and minor elements in aluminium alloys', *Applied Spectroscopy*, vol. 61, no. 3, pp. 327–332, 2007, doi: 10.1366/000370207780220813.

Electronic copy available at: https://ssrn.com/abstract=4284144

[45] C. Sun *et al.*, 'Machine Learning Allows Calibration Models to Predict Trace Element Concentration in Soils with Generalized LIBS Spectra', *Scientific Reports*, vol. 9, no. 1, p. 11363, Aug. 2019, doi: 10.1038/s41598-019-47751-y.
[46] S. A. Davari and D. Mukherjee, 'Deep Learning Models for Data-Driven Laser Induced Breakdown Spectroscopy (LIBS) Analysis of Interstitial Oxygen Impurities in Czochralski-Si Crystals', *Appl Spectrosc*, vol. 76, no. 6, pp. 667–677, Jun. 2022, doi: 10.1177/00037028221085640.
[47] P. Seidel *et al.*, 'Comparison of Elemental Analysis Techniques for the Characterization of Commercial Alloys', *Metals*, vol. 11, no. 5, Apr. 2021, doi: 10.3390/met11050736.
[48] J. Guezenoc, A. Gallet-Budynek, and B. Bousquet, 'Critical review and advices on spectral-based normalization methods for LIBS quantitative analysis', *Spectrochimica Acta Part B: Atomic Spectroscopy*, vol. 160, p. 105688, 2019.
[49] E. D'Andrea *et al.*, 'An artificial neural network approach to laser-induced breakdown spectroscopy quantitative analysis', *Spectrochimica Acta Part B: Atomic Spectroscopy*, vol. 99, pp. 52–58, 2014.
[50] Y. Zhao *et al.*, 'Deep learning associated with laser-induced breakdown spectroscopy (LIBS) for the prediction of lead in soil', *Applied spectroscopy*, vol. 73, no. 5, pp. 565–573, 2019.
[51] J. Castorena, D. Oyen, A. Ollila, C. Legget, and N. Lanza, 'Deep spectral CNN for laser induced breakdown spectroscopy', *Spectrochimica Acta Part B: Atomic Spectroscopy*, vol. 178, p. 106125, 2021.
[52] D. W. Hahn and N. Omenetto, 'Laser-Induced Breakdown Spectroscopy (LIBS), Part II: Review of Instrumental and Methodological Approaches to Material Analysis and Applications to Different Fields', *Applied Spectroscopy*, vol. 66, no. 4, Art. no. 4, 2012.
[53] P. H. C. Eilers and H. F. M. Boelens, 'Baseline correction with asymmetric least squares smoothing', *Leiden University Medical Centre Report*, vol. 1, 2005.
[54] D. F. Andrews, 'A robust method for multiple linear regression', *Technometrics*, vol. 16, no. 4, pp. 523–531, 1974.
[55] C. A. Seybold, M. A. Elrashidi, and R. J. Engel, 'Linear regression models to estimate soil liquid limit and plasticity index from basic soil properties', *Soil science*, vol. 173, no. 1, pp. 25–34, 2008.
[56] A. Kramida, K. Olsen, and Y. Ralchenko, 'NIST LIBS Database'. [Online]. Available: https://physics.nist.gov/PhysRefData/ASD/LIBS/libs-form.html
[57] D. Syvilay, J. Guezenoc, and B. Bousquet, 'Guideline for increasing the analysis quality in laser-induced breakdown spectroscopy', *Spectrochimica Acta Part B: Atomic Spectroscopy*, vol. 161, Nov. 2019, doi: 10.1016/j.sab.2019.105696.
[58] L. Breiman, 'Random forests', *Machine learning*, vol. 45, no. 1, pp. 5–32, 2001.
[59] F. Pedregosa *et al.*, 'Scikit-learn: Machine learning in Python', *the Journal of machine Learning research*, vol. 12, pp. 2825–2830, 2011.
[60] C. Sun *et al.*, 'Machine learning allows calibration models to predict trace element concentration in soils with generalized LIBS spectra', *Scientific reports*, vol. 9, no. 1, pp. 1–18, 2019.
[61] M. Guo, A. Haque, D.-A. Huang, S. Yeung, and L. Fei-Fei, 'Dynamic task prioritization for multitask learning', in *Proceedings of the European conference on computer vision (ECCV)*, 2018, pp. 270–287.
[62] A. Dosovitskiy and J. Djolonga, 'You only train once: Loss-conditional training of deep networks', 2019.
[63] A. BenTaieb and G. Hamarneh, 'Uncertainty driven multi-loss fully convolutional networks for histopathology', in *Intravascular Imaging and Computer Assisted Stenting, and Large-Scale Annotation of Biomedical Data and Expert Label Synthesis*, Springer, 2017, pp. 155–163.
[64] K. Han, Y. Wang, Q. Tian, J. Guo, C. Xu, and C. Xu, 'Ghostnet: More features from cheap operations', in *Proceedings of the IEEE/CVF Conference on Computer Vision and Pattern Recognition*, 2020, pp. 1580–1589.
[65] X. Glorot, A. Bordes, and Y. Bengio, 'Deep sparse rectifier neural networks', in *Proceedings of the fourteenth international conference on artificial intelligence and statistics*, 2011, pp. 315–323.

Electronic copy available at: https://ssrn.com/abstract=4284144

[66] A. Paszke *et al.*, 'Pytorch: An imperative style, high-performance deep learning library', *arXiv preprint arXiv:1912.01703*, 2019.
[67] L. Perez and J. Wang, 'The effectiveness of data augmentation in image classification using deep learning', *arXiv preprint arXiv:1712.04621*, 2017.
[68] C. M. Bishop, 'Pattern recognition and machine learning-springer 2006', *Reference Source*, 2006.
[69] D. P. Kingma and J. Ba, 'Adam: A method for stochastic optimization', *arXiv preprint arXiv:1412.6980*, 2014.

Electronic copy available at: https://ssrn.com/abstract=4284144